Robust Controller Synthesis for a Large Flexible Space Antenna

N. Sundararajan*
Old Dominion University Research Foundation, Norfolk, Virginia
and
S. M. Joshi† and E. S. Armstrong‡
NASA Langley Research Center, Hampton, Virginia

The linear-quadratic Gaussian/loop-transfer-recovery method is used to synthesize a fine-pointing control system for a large space antenna. A finite-element model for the 122-m hoop/column antenna is employed, and a compensator, utilizing attitude sensors and torque actuators, is designed which achieves pointing performance while maintaining stability robustness to unmodeled dynamics. Inclusion of the rigid-body modes plus the first three elastic modes is found to be necessary to achieve a 0.1-rad/s bandwidth. Results are obtained by employing a modification of the standard robustness recovery procedure, which reduces the conservative nature of the design methodology. Performance degradation is encountered due to the presence of unavoidable invariant zeros within the design bandwidth.

I. Introduction

ONE of the planned activities of NASA's Space Transportation System is the placement in Earth orbit of a variety of large space antennas. Potential space missions are expected to require antennas and structures ranging from 30 m to 20 km in size. Applications include communications (mobile), remote sensing (soil moisture, salinity, etc.), deep space network (orbital relays), astronomy (x-ray, observatory, optical array, radio telescope, very long baseline interferometry, etc.), energy, and space platforms. Specific missions have been pinpointed and future requirements have been identified for large space antennas for communications, Earth sensing, and radio astronomy.[1] Particular emphasis is placed on mesh-deployable antennas in the 50–120-m-diam category. One such antenna is the Maypole (hoop/column) antenna, shown schematically in Fig. 1, which basically consists of a deployable central mast attached to a deployable hoop by cables held in tension.[2] The deployable mast consists of a number of telescoping sections, and the hoop consists of 48 rigid segments. The reflective mesh, which is made of knit gold-plated molybdenum wire, is attached to the hoop by graphite fibers. The mesh is shaped using a network of stringers and ties to form the radio-frequency (rf) reflective surface. In order to achieve required rf performance, the hoop/column antenna must be controlled to specific precision in attitude and shape. For example, in missions such as the land mobile satellite system (LMSS) for providing mobile telephone service to users in the continental United States; it is necessary to achieve a pointing accuracy of 0.03 deg rms (root mean square) and a surface accuracy of 6 mm rms. It is also necessary to have stringent control on the motion of the feed (located near one end of the mast) relative to the mesh. Because of its large size and relatively light weight, the antenna is highly flexible with a large number of significant elastic modes. Dynamic equations used to model the structure mathematically have many resonant frequencies, some of which may be very low and closely spaced, and natural damping is very small. For these reasons, control of large space structures is a challenging task.[3] Since the system is inherently of high order, a practical controller has to be based on a reduced-order "design" model. Furthermore, the parameters (i.e., frequencies, mode shapes, and damping ratios) of the system are known imprecisely. This, in turn, introduces additional modeling errors.

Reduced-order control synthesis for the hoop/column antenna using the standard linear-quadratic-Gaussian (LQG) theory was investigated in Refs. 4 and 5. The standard LQG procedure yielded satisfactory control, i.e., rigid-body bandwidth of up to 0.25 rad/s, satisfactory time constants for the elastic modes, and acceptable rms pointing errors in the presence of sensor noise. However, the LQG approach in Ref. 4 used a large number of actuators and sensors (four three-axis torque actuators and four three-axis attitude and rate sensors). The main problem with the LQG method was that a large number of weighting parameters had to be simultaneously adjusted to obtain a good design. In addition, the stability robustness property with respect to inaccuracies in the modal parameters could not be properly evaluated because it was difficult to characterize effectively the bounds on modeling errors in a time-domain setting. In order to reduce these difficulties, one normally checks the control design for robustness after the control design is completed using LQG or any other method. Attempts have been made to characterize bounds on parameter uncertainty in a time-domain setting (see, for example, Ref. 6). However, meaningful time-domain characterization of simultaneous errors in model order and parameter uncertainties is still an open area of research. Another approach is to use frequency-domain characterization of modeling errors. Such an approach using frequency-domain singular-value measures was presented in Ref. 7 for a large space structure using different control design methods, such as LQG, integral feedback, frequency-shaped LQG, etc.

Submitted Nov. 20, 1985; revision submitted June 13, 1986.

*Associate Professor (Research); presently with Indian Space Research Organization, Bangalore, India. Senior Member AIAA.
†Senior Research Scientist, Guidance and Control Division. Associate Fellow AIAA.
‡Senior Research Scientist, Guidance and Control Division.

Unlike the foregoing methods, the linear-quadratic-Gaussian/loop-transfer-recovery (LQG/LTR) approach provides a means of including robustness-to-uncertainties in the control design process itself. Also, since it operates in the frequency domain, it extends the basic frequency-domain design guidelines, such as bandwidth, crossover frequency, etc., from a scalar system to a multivariable system.

The robust control synthesis methodology, which uses frequency-domain matrix norm bounds (i.e., singular values), has received considerable attention in the recent literature.[8-13] The basic framework for frequency-domain synthesis using the LQG/LTR methodology was developed in Refs. 8–10. It has been applied to diverse systems, such as power systems,[11] aircraft control,[12] and aircraft engine control.[13] The LQG/LTR design philosophy uses a low-frequency "design model" of the plant and a high-frequency characterization of the modeling errors. This method, which characterizes unstructured uncertainty with singular-value bounds, appears to be particularly well suited for the control of large flexible spacecraft due to the considerable modeling inaccuracy that inherently exists in the mathematical models.

The purpose of this paper is to investigate the use of LQG/LTR multivariable frequency-domain methodology in the design of an attitude control system for the hoop/column antenna. A low-order compensator is obtained by treating a sequence of finite-element design models ordered with increasing modal frequency and choosing the final design model as the first one which allows the performance/robustness objectives to be met. In this sequence of design models, the first one consists of the rigid-body modes only. Subsequent design models are obtained by the successive addition of flexible modes. The designs use three-axis torque actuators, collocated attitude sensors, and attitude feedback.

The organization of this paper is as follows: The mathematical model of the system is described in Sec. II. The control objective is briefly discussed in Sec. III, followed by a brief description of the LQG/LTR technique in Sec. IV. The reduced-order (low-frequency) design model and the high-frequency model uncertainty barrier are also discussed in this section. Section V presents the results of synthesizing the controller based on the preceding procedure using only attitude feedback. Some of the problems and limitations observed are also highlighted. Based on the study results, the conclusions are summarized in Sec. VI.

II. Mathematical Model

As a consequence of its large size and light weight, the hoop/column antenna is a highly flexible system having a large number of significant structural modes. A finite-element model of the antenna[2] is used herein. The mathematical model considered consists of rotational rigid-body dynamics (about the three axes) and the elastic motion. It is assumed here that control will be accomplished by using n_T three-axis torque actuators. The linearized equations of motion are

$$I_s\ddot{\alpha} = \sum_{j=1}^{n_T} T_j \tag{1}$$

$$\ddot{q} + D\dot{q} + \Lambda q = \Phi^T u \tag{2}$$

where I_s is the 3×3 inertia matrix, T_j is the three-axis torque applied by the jth actuator, $\alpha_s = (\phi_s,\ \theta_s,\ \psi_s)^T$ denotes the rigid-body attitude, q is the $n_q \times 1$ modal amplitude vector (for n_q structural modes), and $D = 2$ diag $(\rho_1\omega_1,\ \rho_2\omega_2,\ \ldots,\ \rho_n\omega_n)$ is the inherent damping matrix (where ρ_i is the damping ratio for the ith mode). Φ is the $m\times n_q$ "mode-slope" matrix (where $m = 3n_T$), $u = (T_1^T,\ T_2^T,\ \ldots,\ T_{n_T}^T)^T$ is the $m\times 1$ vector of actuator torques, and $\Lambda =$ diag $(\omega_1^2,\ \omega_2^2,\ \ldots,\ \omega_{n_q}^2)$, where ω_i is the frequency of the ith elastic mode. The rigid-body parameters and the first ten elastic frequencies are given in Table 1. Each ρ_i is assumed to be 0.01 for $i = 1, 2, \ldots, n$.

Normally, the sensors used include attitude and rate sensors. The three-axis attitude sensor (e.g., a star tracker) output is given by

$$y_a = \alpha_s + \psi q + w \tag{3}$$

where ψ is the $3\times n_q$ mode-slope matrix at the sensor location and w is the sensor noise. If an attitude rate sensor (e.g., a rate gyro) is used, the sensor output y_r is given by an equation similar to Eq. (3), except that α_s and q are replaced by $\dot{\alpha}_s$ and $\dot{q}$, respectively. Torque actuators and attitude sensors are assumed to be located near the top of the mast at the antenna feed (Fig. 1).

Defining $x = (\alpha_s^T,\ \dot{\alpha}_s^T,\ q^T,\ \dot{q}^T)^T$ as an $n\times 1$ vector, the state space model can be written in the following form:

$$\dot{x} = A_F x + B_F u \tag{4}$$

$$y = C_F x + w \tag{5}$$

The sensor noise w is not used in the design process in this paper; however, it will have to be included when computing the rms pointing errors. Ignoring the noise, the transfer matrix between the input (three-axis torque) and output three-axis attitude) is given by

$$G(s) = G_1(s) + G_2(s) \tag{6}$$

where

$$G_1(s) = I_S^{-1}/s^2 \tag{7}$$

$$G_2(s) = \sum_{i=1}^{n_q} (\psi_i\phi_i^T)/(s^2 + 2\rho_i\omega_i s + \omega_i^2) \tag{8}$$

ψ_i and ϕ_i represent the mode-slope matrices at the sensor and actuator locations corresponding to the ith mode.

Table 1 Antenna parameters

Rigid-body parameters Mass = 4544.3 kg
Inertia about axes through center of mass, kg-m^2 $I_{xx} = 5.724\times 10^6$ $\quad I_{yy} = 5.747\times 10^6$ $I_{zz} = 4.383\times 10^6$ $\quad I_{yz} = I_{xz} = I_{xy} = 0$
Structural mode frequencies, rad/s 0.75, 1.35, 1.7, 3.18, 4.53, 5.59, 5.78, 6.84, 7.4, 8.78

Table 2 Eigenvalues of the full closed-loop system

$-8.535\times 10^{-3} \pm j8.054\times 10^{-2}$
$-7.557\times 10^{-2} \pm j1.250\times 10^{-1}$
$-7.604\times 10^{-2} \pm j1.248\times 10^{-1}$
$-2.237\times 10^{-1} \pm j2.236\times 10^{-1}$
$-2.330\times 10^{-1} \pm j2.154\times 10^{-1}$
$-2.379\times 10^{-1} \pm j2.113\times 10^{-1}$
$-7.466\times 10^{-3} \pm j7.466\times 10^{-1}$
$-1.346\times 10^{-2} \pm j1.346$
$-3.076\times 10^{-1} \pm j1.373$
$-1.016 \pm j1.267$
$-1.702\times 10^{-2} \pm j1.702$
$-4.028\times 10^{-1} \pm j1.737$
$-3.181\times 10^{-2} \pm j3.181$
$-4.422\times 10^{-2} \pm j4.529$
$-5.579\times 10^{-2} \pm j5.590$
$-5.731\times 10^{-2} \pm j5.776$
$-6.685\times 10^{-2} \pm j6.841$
$-6.390\times 10^{-2} \pm j7.401$
$-8.326\times 10^{-2} \pm j8.782$

III. Design Objectives

The basic design objectives for the control systems are: 1) to obtain sufficiently high bandwidth (i.e., closed-loop frequencies corresponding to the rigid-body modes) and satisfactory closed-loop damping ratios for the rigid-body and structural modes; and 2) to obtain satisfactory rms pointing errors, feed motion errors, and surface errors. The first design objective arises from the need to obtain sufficiently fast error delay when a step disturbance (such as sudden thermal distortion caused by entering or leaving Earth's shadow) occurs. The second design objective arises from the rf performance requirements. These two objectives may not necessarily be compatible, and may even be conflicting. For example, the use of increased feedback gains for obtaining higher bandwidth and damping ratios will, in general, result in higher rms errors (because of the amplified effect of sensor noise) beyond a certain point. Therefore, it is necessary to consider carefully the tradeoffs between the speed of response and lower rms error. In this study, the main control system specification is that a minimum bandwidth of 0.1 rad/s for the closed-loop system is to be ensured. The upper limit on the low-frequency gain is not specified, but it is desired that it should be as high as possible. Also, for this study no specification on rms errors was made; this aspect along with measurement noise will be considered in the future.

IV. Design Procedure

The LQG/LTR method has been described in detail in Refs. 8–10. A tutorial description and an example application are given in Ref. 12. Here, the main steps are summarized first and then each step is discussed in detail.

1) Define a "design" model of the nominal plant, which is an acceptable low-frequency representation. Define the high-frequency uncertainty (robustness) barrier and the low-frequency performance barrier.

2) Design a full state feedback compensator based on the steady-state Kalman-Bucy filter (KBF). This assumes that the loop is broken at the output. Adjust the weighting matrices in the KBF design until its frequency response meets the robustness specifications at high frequencies and bandwidth specification at low frequencies.

3) Design a LQ regulator to "recover" asymptotically the frequency response obtained in step 2.

4) Verify stability, robustness, and performance for the entire closed-loop system.

The first step, which consists of the definition of the plant and the uncertainty (robustness) barrier, is often the most important. The basic problem in controlling a flexible structure is the presence of a large number of lightly damped structural modes. Practical limitations necessitate the use of reduced-order controllers. Therefore, the uncontrolled modes, as well as the error in the knowledge of the controlled modes, represent uncertainty. Since the number of structural modes is usually large and finite-element modeling accuracy typically decreases with increasing model frequency, the design model should consist of the rigid-body mode plus the first few elastic modes. The remaining structural modes then (partly) constitute the plant uncertainty. In order to obtain an acceptable low-frequency representation, the design model must include at least the three rigid-body modes. The uncertainty barrier is a measure of the plant uncertainty at high frequencies. The plant uncertainty can be represented as either multiplicative or additive uncertainty (Fig. 2). The multiplicative uncertainty form is preferred in the literature on robustness because the compensated transfer function has the same uncertainty representation as the raw model. However, since flexible structure models exhibit naturally the additive uncertainty form of the transfer function matrix, this will be used in the following studies. The LQG/LTR approach required the characterization of the uncertainty in terms of a frequency-dependent upper bound. Frequency-domain sufficient conditions are used to test the robustness in the presence of uncertainties within that bound.

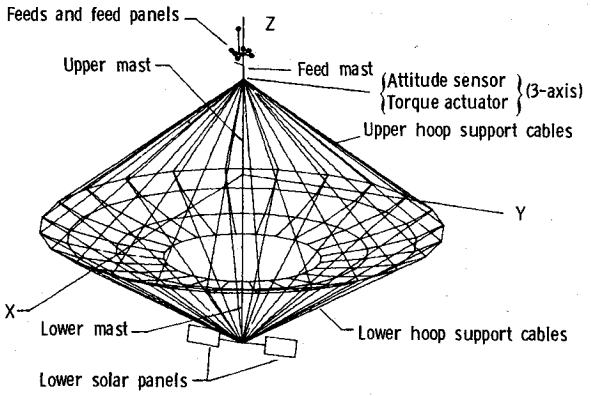

Fig. 1 Hoop/column antenna concept.

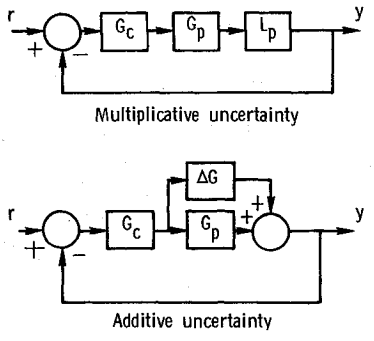

Fig. 2 Definition of uncertainty.

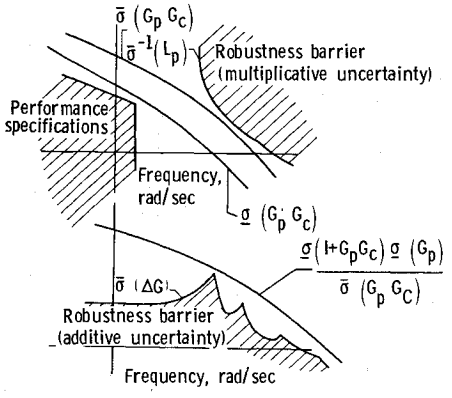

Fig. 3 Performance and robustness barriers.

For the case of multiplicative uncertainty, $L_p(s)$ of Fig. 2, the closed-loop system is stable if

$$\bar{\sigma}[L_p(j\omega) - 1] \leq \underline{\sigma}[I + (G_p(j\omega)G_c(j\omega))^{-1}] \tag{9}$$

where $G_p(s)$ and $G_c(s)$ are the design model (plant) and compensator transfer matrices, and $\bar{\sigma}$ and $\underline{\sigma}$ denote the largest and the smallest singular values of the argument matrix, respectively. At high frequencies, assuming $\|[L_p(j\omega)]\| \gg 1$ and $\|[G_p(j\omega)G_c(j\omega)]\| \ll 1$, condition (9) approximately yields

$$\bar{\sigma}(G_p G_c) < \frac{1}{\bar{\sigma}(L_p)} \tag{10}$$

The "uncertainty (or robustness) barrier" is an upper bound $\ell_m(\omega)$ on $\bar{\sigma}(L_p)$. The system is stable in the presence of such

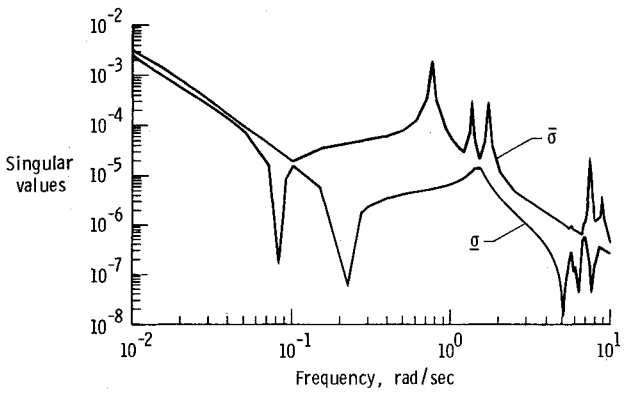

Fig. 4 Singular values of full nominal plant.

unstructured uncertainties if $\bar{\sigma}[G_pG_c] < \ell_m^{-1}(\omega)$ at high frequencies.

When the additive uncertainty formulation (Fig. 2) is used, a sufficient condition for stability robustness is given by[14]

$$\frac{\underline{\sigma}(I+G_pG_c)}{\bar{\sigma}(G_c)} > \bar{\sigma}(\Delta G) \tag{11}$$

At high frequencies, assuming $\|G_pG_c\| \ll 1$, Eq. (11) (approximately) yields

$$\bar{\sigma}(G_c) < 1/\bar{\sigma}(\Delta G) \tag{12}$$

That is, the compensator must roll off sufficiently rapidly at high frequencies. The main objective of the LQG/LTR approach is to first design a full state compensator (based on KBF) which has the behavior of the desired loop transfer matrix (i.e., the loop gain G_pG_c). Therefore, (from step 2) any loop shaping should involve the product G_pG_c rather than G_c alone as in Eqs. (11) and (12). Assuming that G_p is a square matrix,

$$G_c = G_p^{-1}(G_pG_c) \tag{13}$$

$$\bar{\sigma}(G_c) \le \bar{\sigma}(G_p^{-1})\bar{\sigma}(G_pG_c)$$

or

$$\bar{\sigma}(G_c) \le \underline{\sigma}^{-1}(G_p)\bar{\sigma}(G_pG_c) \tag{14}$$

Using Eqs. (11) and (14), the following sufficient condition for stability robustness is obtained:

$$\frac{\underline{\sigma}(I+G_pG_c)\underline{\sigma}(G_p)}{\bar{\sigma}(G_pG_c)} > \bar{\sigma}(\Delta G) \tag{15}$$

The second step in the design procedure is to design a full state feedback compensator having desirable singular-value properties. The performance of the closed-loop system depends on the low-frequency gain and the crossover frequency of the loop transfer matrix G_pG_c; that is, on the behavior of $\underline{\sigma}[G_pG_c]$. Larger low-frequency gain and crossover frequency indicate better tracking performance. Thus, $\underline{\sigma}[G_pG_c]$ should lie above the performance specification, as shown in Fig. 3. The other requirement is the stability robustness in the presence of model uncertainties. If the multiplicative uncertainty formulation is used, according to Eq. (10), the $\bar{\sigma}[G_pG_c]$ plot should pass under the robustness barrier $\bar{\sigma}^{-1}(L_p)$ at high frequencies (Fig. 3). On the other hand, if the additive formulation is used, the robustness condition (15) should be satisfied (Fig. 3). The advantage of an LQG-based full state design is that it has excellent classical properties, and its frequency response can be shaped in the desired manner (to satisfy both performance and robustness specifications) by varying the weighting matrices.[9] As discussed in Ref. 8, this design can be accomplished using the LQR Riccati equation if the loop is broken at the plant input, or the KBF Riccati equation if it is broken at the point where the residual signal enters the KBF. Herein we select the latter because the objective is to control the attitude output. This selection is also consistent with Refs. 10–13. The KBF equations are

$$A\Sigma + \Sigma A^T + LL^T - (1/\mu)\Sigma CC^T\Sigma = 0 \tag{16}$$

and

$$H - (1/\mu)\Sigma C^T \tag{17}$$

where L and μ are the design parameters, L being an $n \times m$ matrix and μ a scalar. The matrix H is the KBF gain and Σ is the corresponding Riccati matrix. The KBF loop transfer matrix is given by

$$G_{KF}(s) = C(sI - A)^{-1}H \tag{18}$$

Generally the frequency response $\sigma(G_{KF}(j\omega))$ would shift higher as μ decreases, and the crossover frequency can be adjusted by changing L.[7]

Having obtained satisfactory singular-value behavior of KBF, the next step is to design an LQR to "recover" the desired frequency response. This is accomplished by solving the algebraic Riccati equation

$$A^TP + PA^T - PBB^TP + qC^TC = 0 \tag{19}$$

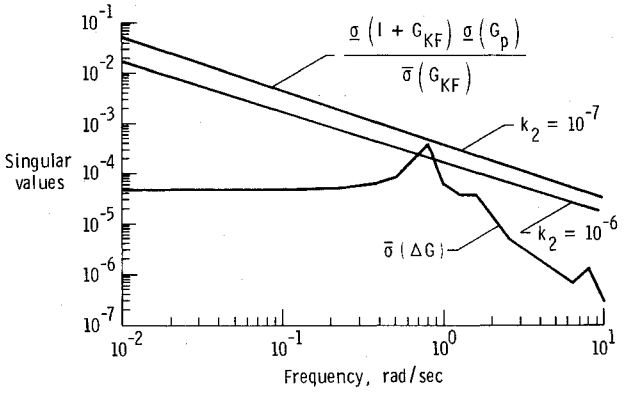

Fig. 5 Stability robustness test [Eq. (15)] for KBF-based loop shaping.

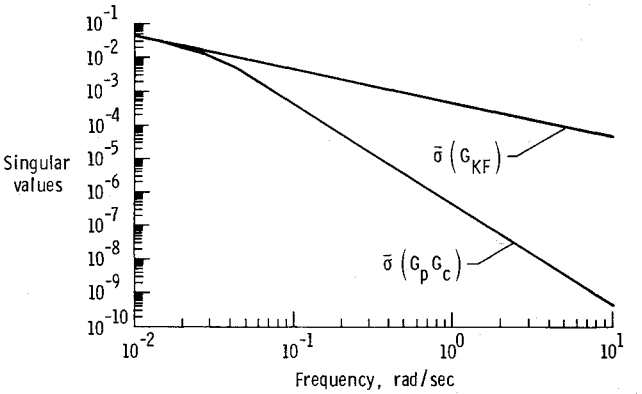

Fig. 6 Singular values of G_{KF} and "recovered" G_pG_c.

where P is the Riccati matrix and q is a positive scalar. The control gain matrix G is given by

$$G = B^T P \tag{20}$$

It has been proven in Refs. 8 and 9 that the loop transfer matrix $G_p G_c$ for the overall system (consisting of the plant, the KBF, and the LQR) tends to $G_{KF}(s)$ as $q \to \infty$, provided that the open-loop plant has no transmission zeros in the right half-plane. The compensator $G_c(s)$, after recovery, is given by

$$G_c(s) = G(sI - A + BG + HC)^{-1} H \tag{21}$$

Since the compensation obtained has no guaranteed robustness properties, the last step will consist of testing the eigenvalues of the entire closed-loop system to ensure stability and robustness. If instability is discovered, it will be necessary to return to step 2 and redesign the KBF for lower bandwidth and the LQR for robustness recovery. If this does not produce satisfactory results, it would then be necessary to return to step 1 and include more elastic modes in the design model. Application of the foregoing LQG/LTR procedure for the hoop/column antenna is described in the following section.

V. Controller Design by the LQG/LTR Method Using Attitude Feedback

The foregoing procedure has been applied to the hoop/column antenna model. The computation of singular values of various matrices (e.g., loop transfer, return difference, inverse return difference matrices) was carried out using a recently developed multivariable frequency-domain analysis software package (FREQ), and the LQG designs were carried out using ORACLS.[15] The nominal plant includes three rotational rigid-body modes and the first ten elastic modes. We assume three torque actuators; hence, the order of B matrix is 26×3. Assuming three attitude sensors (one for each axis) at the same location as the actuators, C is a 3×26 matrix. The plant, input, and output matrices were obtained from a finite-element analysis of the antenna.

Before starting the controller design, the maximum and minimum singular values ($\bar{\sigma}$ and $\underline{\sigma}$) of the full, nominal, open-loop plant transfer matrix were obtained and are shown in Fig. 4. The σ-plot clearly shows the peaks at the elastic mode frequencies (i.e., the poles), the most prominent being the first mode near 0.75 rad/s. The dips in $\underline{\sigma}$ indicate the presence of transmission zeros for the multivariable plant at those frequencies. The controller synthesis studies are performed using the design model consisting of 1) the rigid-body model ($n=6$, $n_q=0$), 2) the rigid-body and the first flexible mode ($n=8$, $n_q=1$), and 3) the rigid-body and the first three flexible modes ($n=12$, $n_q=3$). The measurements available are the three attitude angles at the feed location. One three-axis torque actuator is used at the same location. The compensator is designed based on these sensors and actuators.

Rigid-Body Model

In this section the controller design is carried out based only on the rigid-body design model. The singular values of the rigid-body transfer matrix ($n=6$) are proportional to $1/s^2$. The corresponding additive uncertainty ΔG, which consists of the (20th-order) flexible dynamics, is plotted in Fig. 5. Figure 5 indicates the presence of poles near the undamped flexible mode frequencies of 0.75, 1.35 rad/s, etc. Also, the pole of the first mode frequency of 0.75 rad/s produces the highest peak since it is most lightly damped. (The importance of this fact will be seen later when the stability condition is violated at this point.)

For this sixth-order design model, a compensator design was carried out using the Kalman filter design methodology to achieve satisfactory performance (i.e., large gain and bandwidth) at low frequencies and robustness at high frequencies. This design was carried out using the Kalman filter Riccati equation (16). The Kalman-Bucy filter transfer matrix $G_{KF}(s)$ is given in Eq. (18). Appropriate loop shaping can be accomplished by proper choice of the weights μ and L in Eq. (16). Since the controller design model is of the form $1/s^2$, one can analytically evaluate the singular values of $I + G_{KF}$ using Eqs. (16) and (17). Assuming $\mu = 1$ and $L = (L_1, L_2)^T$, the left-hand side of condition (15) can be evaluated. For $L_1 = 0$ and $L_2 = k_2 I$, it can be shown that Eq. (15) is satisfied with $k_2 < 10^{-7}$. This implies that the Kalman filter gain computed using Eq. (17) will be very low. Figure 5 shows plots for condition (15) with two L matrices generated by $L_1 = 0$ and $k_2 = 10^{-6}$ and 10^{-7}. The right-hand side of Eq. (15) is also plotted in Fig. 5. It is evident that condition (15) is satisfied for $k_2 = 10^{-7}$. As k_2 is decreased further, the curve shifts upward thus increasing the margin.

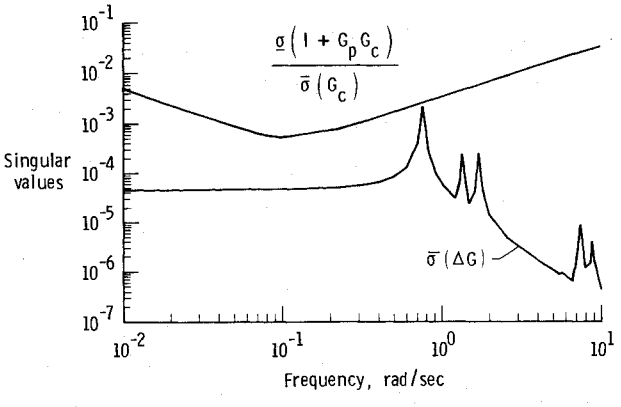

Fig. 7 Stability robustness test [Eq. (11)] based on the recovered compensator.

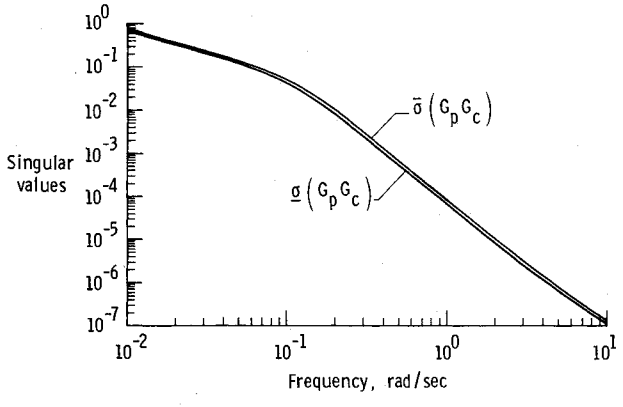

Fig. 8 Singular values of recovered loop transfer matrix $G_p G_c$.

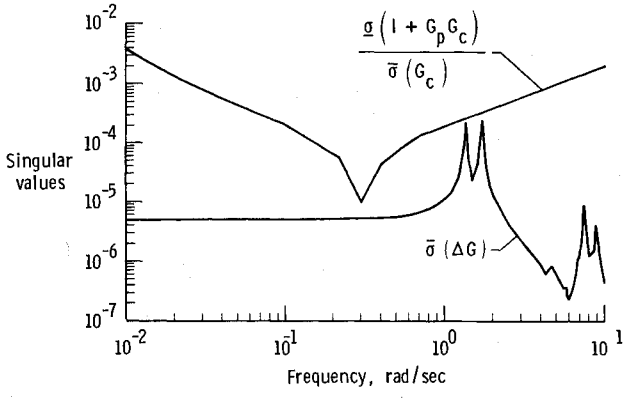

Fig. 9 Stability robustness test [Eq. (11)] for one-mode model.

The next step consists of LQ regulator design. Having obtained an acceptable compensator through Kalman-Bucy filter equations, the LQ regulator is realized via the loop transfer recovery method.[9] Singular-value plots of the complete loop transfer matrix $G_pG_c(s)$ (which consist of the plant, the KBF, and the LQR) were made for different values of the weighting parameter q [Eq. (19)]. The selected value was $q=10^6$ with resulting $\bar{\sigma}$ shown in Fig. 6. It is easy to check condition (11) in this case. As q is increased, the plots approach those of the compensator obtained from the Kalman filter design approach. The LQR design for $q=10^6$ was considered to be satisfactory.

The standard LQG/LTR procedure requires the definition of the "desired" loop transfer characteristics (see step 2 in Sect. III). That is, $\underline{\sigma}(G_{KF})$ must satisfy the low-frequency performance specifiations, and $\bar{\sigma}(G_{KF})$ must satisfy the high-frequency robustness specifications. Thus, in the presence of additive uncertainty ΔG, the procedure states that the robustness condition

$$\frac{\underline{\sigma}(I+G_{KF})\underline{\sigma}(G_p)}{\bar{\sigma}(G_{KF})} > \bar{\sigma}(\Delta G) \tag{22}$$

should be satisfied. However, in the case described previously, it was found that the preceding condition makes the "desired" design (G_{KF}) extremely conservative. From Fig. 6, it is seen that the closed-loop bandwidth is quite low and nowhere near the desired value of 0.1 rad/s. Therefore, recovering this conservative loop gain yields a compensator with poor performance. This fact led to a modification of the LQG/LTR procedure. In particular, the preceding robustness test on G_{KF} is omitted in the modified procedure. Instead, the recovery is carried out first, and then the (less conservative) stability test [Eq. (11)] is applied directly for the compensator G_c. The Kalman filter transfer matrix G_{KF} is based only on the desired performance and not on satisfying the stability test of Eq. (15). With the revised test on G_c, the following choices of L and μ were

$$L=\begin{bmatrix} 0 \\ \hline 10^{-2}I \end{bmatrix}; \qquad \mu=1 \tag{23}$$

Using the recovery procedure, the compensator is obtained for this case with $q=10^4$. The resulting stability test [Eq. (11)] is shown in Fig. 7. It is seen that the stability margin is lowest at the first mode frequency (0.75 rad/s). Any increase in the gain (obtained by $q>10^4$) resulted in violation of stability condition at that point. The overall loop bandwidth is obtained from the singular values of the loop transfer function G_pG_c shown in Fig. 8. It is seen that the bandwidth [i.e., the frequency at which $\underline{\sigma}(G_pG_c)=1$] is far short of the required 0.1 rad/s. In order to increase the bandwidth, the gain has to be increased by increasing q. However, this results in the violation of the stability condition (11). Thus it is evident that, with a rigid-body design model, it is not possible to meet the performance specifications.

One-Flexible-Mode Design Model

To overcome the preceding problems, the next alternative considered was whether the inclusion of the first flexible mode (0.75 rad/s) in the design model would improve the performance. The inclusion of the first flexible mode, which is predominantly a torsion mode, results in a design model of order 8. The singular value $\bar{\sigma}$ of ΔG shown in Fig. 9 is an order of magnitude lower than that in Fig. 5 (wherein ΔG consisted of *all* the flexible modes). The first peak of $\sigma(\Delta G)$ occurs at 1.35 rad/s, which is the frequency of the second mode. This is the critical point in the stability test [Eq. (11)]. After a number of trials, the following choice of L and μ was made to obtain the desired performance G_{KF}.

$$L=\begin{bmatrix} 0 \\ \hline 10^{-2}I_3 \\ \hline 10^{-2}I_2 \quad 0 \end{bmatrix}; \qquad \mu=1 \tag{24}$$

The recovery is obtained for $q=10^5$ and the stability test is shown in Fig. 9. Figure 9 indicates the critical point to be at about 0.28 rad/s. There is a good margin at the peaks of ΔG due to upward sloping of the upper curve. The resulting loop transfer function (G_pG_c) plots are shown in Fig. 10. The plots indicate that the required 0.1-rad/s bandwidth is not obtained (although it is much higher than the rigid-model case). Any increase in the gain (for $q>10^5$) was found to result in the violation of the stability condition (11). Figure 10 indicates that

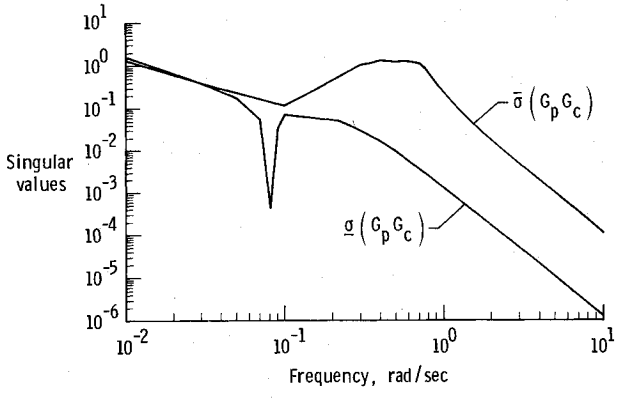

Fig. 10 Singular values of G_pG_c for one-mode model.

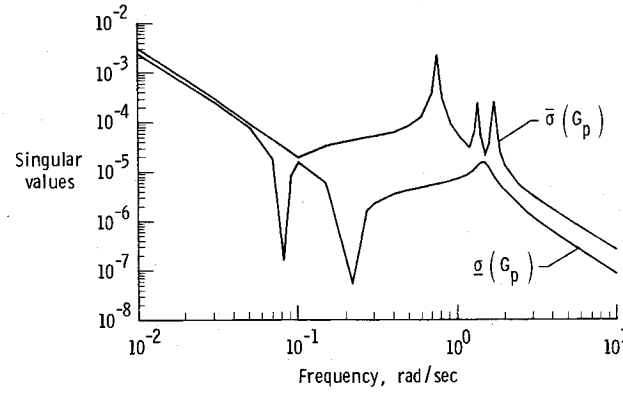

Fig. 11 Singular values of G_p for three-mode model.

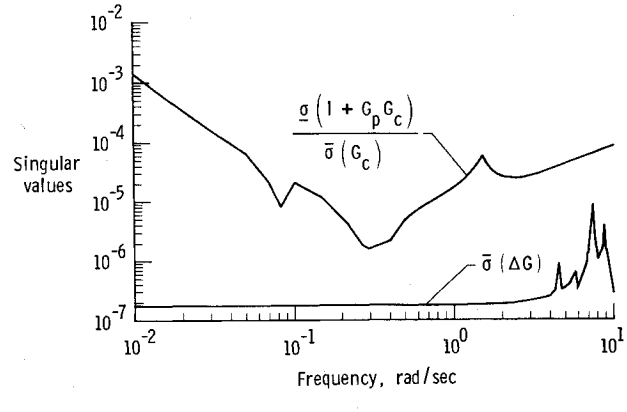

Fig. 12 Stability robustness test [Eq. (11)] for three-mode model.

presence of an open-loop invariant zero near 0.082 rad/s, which was also confirmed by independent computations. This zero is almost on the imaginary axis (i.e., the transfer matrix is close to being nonminimum phase). Therefore, as would be expected, the recovery procedure is not very effective for making G_pG_c approximate G_{KF}.

Three-Flexible-Mode Design Model

In order to improve the performance further, the next step was to include the first three flexible modes in the design model. It is logical to do this because they represent the first modes about each axis, i.e., the first torsion mode and the first bending modes in the XZ and YZ planes. Thus, the order of the design model was 12. The singular-value plots for G_p and ΔG are shown in Figs. 11 and 12, respectively. It is seen from Fig. 11 that G_p has zeros near 0.082 and 0.22 rad/s, and poles near 0.75, 1.35, and 1.7 rad/s. It is seen from the ΔG plot (Fig. 12) that $\bar{\sigma}$ is considerably lower than that in Figs. 7 and 9. After numerous trials, the following choice of the L matrix and the scalar μ was made for a suitable G_{KF}:

$$L=\begin{bmatrix} 0 \\ \hline 10^{-1}I_3 \\ \hline 10^{-4}I_2 \quad 0 \\ \hline 10^{-4}I_2 \quad 0 \\ \hline 10^{-4}I_2 \quad 0 \end{bmatrix}; \qquad \mu=1 \tag{25}$$

The recovery was accomplished with $q=10^{10}$. The stability test is shown in Fig. 12. It can be seen that condition (11) is satisfied with a wide margin. Also, at the peak for ΔG (at 8 rad/s) the upper curve slopes upward, indicating good tolerance of high-frequency uncertainty. The limit for increasing the gain (indicated by the lowest point in the upper curve in Fig. 12) occurs at about 0.3 rad/s. The resulting compensator G_c is shown in Fig. 13. The gain of G_c is much higher than that obtained in the previous cases. Generally, the LQG/LTR technique attempts to choose G_c in such a way that the product G_pG_c is replaced by G_{KF} (i.e., is attempting to invert G_p in the frequency range of interest). The three-mode design plant shown in Fig. 11 has elastic mode eigenvalues at $-0.0075 \pm j0.75$, $-0.0135 \pm j1.35$, and $-0.0170 \pm j1.70$. Figure 13 shows that G_c has zeros with frequencies near these locations. The design plant also has transmission zeros at $-0.9\times10^{-4} \pm j0.082$, $-0.37\times10^{-3} \pm j0.22$, and $-0.29\times10^{-3} \pm j0.22$, which are retained by G_c. The plots for the loop transfer matrix G_pG_c are given in Fig. 14. It is seen that a bandwidth of 0.1 rad/s is obtained except for the presence of the invariant zero near 0.082 rad/s, which causes some deterioration of performance. At frequencies past 0.4 rad/s G_pG_c behaves likes G_{KF} and eventually rolls off at 60 dB/decade. Also, $\underline{\sigma}$ and $\bar{\sigma}$ are closely spaced, indicating good system behavior. Thus is it seen that inclusion of the first three modes in the design model yields a robust compensator which also meets the bandwidth specifications.

The final step is to check the stability of the complete nominal system when the compensator $G_c(s)$ designed previously is used. The overall closed-loop system is

$$\begin{bmatrix} \dot{x} \\ \dot{\hat{x}} \end{bmatrix} = \begin{bmatrix} A_F & -B_FG \\ HC_F & A-BG-HC \end{bmatrix} \begin{bmatrix} x \\ \hat{x} \end{bmatrix} \tag{26}$$

where the subscript F is used to denote the full-order nominal plant, and x denotes the state estimate for the design model. The eigenvalues of the overall closed-loop system using the three-mode controller are given in Table 2. It can be seen from Table 2 that the overall closed-loop system is stable.

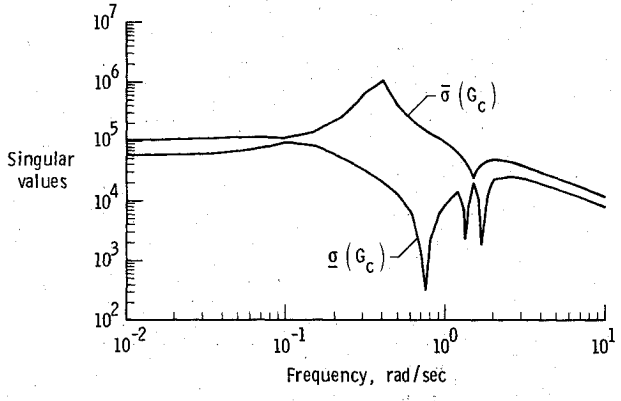

Fig. 13 Singular values of the compensator G_c for three-mode model.

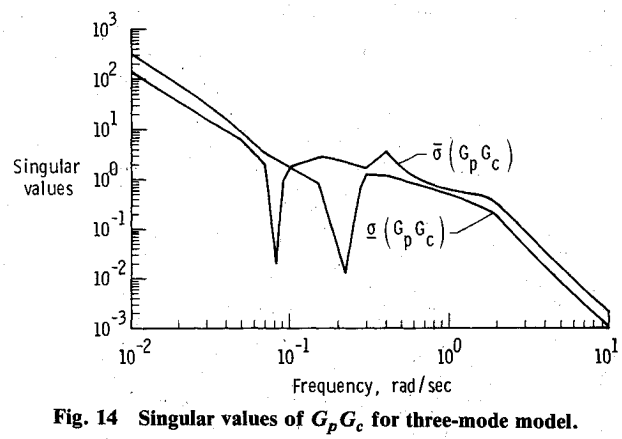

Fig. 14 Singular values of G_pG_c for three-mode model.

VI. Concluding Remarks

The linear-quadratic-Gaussian/loop-transfer-recovery multivariable frequency-domain technique was employed in the design of an attitude control system for a large flexible space antenna. This approach was noted to be useful for alleviating spillover effects common to large-space-structures control problems modeled from finite-element data. The design objective of avoiding excitation of higher-order modes while satisfying performance criteria was met by including these modes in the robustness uncertainty barrier.

Design was based on a reduced-order model chosen as the rigid-body dynamics plus the fewest number of low-frequency vibrational modes necessary to meet a desired closed-loop bandwidth. Inclusion of the first three vibrational modes (corresponding to the three axes) was found to be necessary to meet a 0.1-rad/s bandwidth. For wider bandwidths, design models with greater than three modes may be needed. A satisfactory control design was obtained using only a collocated single pair of three-axis attitude sensor and torque actuator for the hoop/column antenna problem.

Performance degradation was observed due to the presence of invariant zeros within the design bandwidth. These zeros were unavoidable given the prescribed sensor/actuator locations and emphasized the fact that consideration should be given to control aspects in the early design phase of large space structures.

A modification of the standard linear-quadratic-Gaussian/loop-transfer-recovery procedure was introduced in which the robustness test was performed with the full compensator instead of the intermediate Kalman filter design. This approach was found to produce higher performance compensators and helped overcome the basic conservativeness shortcoming of the linear-quadratic-Gaussian/loop-transfer-recovery approach.

References

[1]Russell, R. A., Campbell, T. G., and Freeland, R. E., "A Technology Development Program for Large Space Antennas," Paper IAF-80A33, Sept. 1980.

[2]Sullivan, M. R., "LSST (Hoop/Column) Maypole Antenna Development Program, Parts I and II," NASA CR-3558, June 1982.

[3]Balas, M. J., "Trends in Large Space Structure Control Theory: Fondest Hopes, Wildest Dreams," *IEEE Transactions on Automatic Control*, Vol. AC-27, June 1982, pp. 552–535.

[4]Joshi, S. M., "Control Systems Synthesis for a Large Flexible Space Antenna," *Acta Astronautica*, Vol. 10, No. 5-6, May 1983, pp. 365–380.

[5]Wang, S. J. and Cameron, J. M., "Dynamics and Control of A Large Space Antenna," *Journal of Guidance, Control, and Dynamics*, Vol. 7, Jan.-Feb. 1984, pp. 69–76.

[6]Yedavalli, R. K., Banda, S. S., and Ridgely, D. B., "Time Domain Stability Robustness Measures for Linear Regulators," *Journal of Guidance, Control, and Dynamics,* Vol. 8, July-Aug. 1985, pp. 520–525.

[7]Kosut, R. L. et al., "Robust Control of Flexible Spacecraft," *Journal of Guidance, Control, and Dynamics*, Vol. 6, March-April 1983, pp. 104–111.

[8]Doyle, J. C. and Stein, G., "Multivariable Feedback Design: Concepts for a Classical/Modern Synthesis," *IEEE Transactions on Automatic Control,* Vol. AC-26, Feb. 1981, pp. 4–16.

[9]Stein, G., "LQG-based Multivariable Design: Frequency Domain Interpretation," *Multivariable Analysis and Design Techniques,* AGARD Lecture Series LS-117, 1981, pp. 5-1–5-9.

[10]Athans, M., "Multivariable Control System Design Using the LQG/LTR Methodology," unpublished lecture notes (lecture given at NASA Langley Research Center) 1984.

[11]Chan, S. M. and Athans, M., "Applications of Robustness Theory to Power System Models," *IEEE Transactions on Automatic Control,* Vol. AC-29, Jan. 1984, pp. 2–8.

[12]Ridgely, D. B. and Banda, S. S., "Introduction to Robust Multivariable Control," AFWAL-TR-85-3102, Feb. 1986.

[13]Kappos, E., "Robust Multivariable Control of the F-100 Engine," MIT, Cambridge, MA, Rept. LIDS-TH-1328, Sept. 1983.

[14]Cruz, J. B. et al., "A Relationship Between Sensitivity and Stability of Multivariable Feedback Systems," *IEEE Transactions on Automatic Control,* Vol. AC-26, Feb. 1981, p. 66–74.

[15]Armstrong, E. S., *ORACLS—A Design System for Linear Multivariable Control*, Marcel & Dekker Control and System Theory Series, Vol. 10, 1980.